N71-10995

NASA TECHNICAL MEMORANDUM

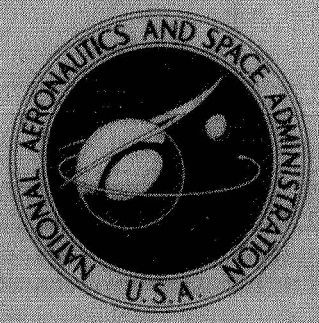

NASA TM X-2084

NASA TM X-2084

CASE FILE COPY

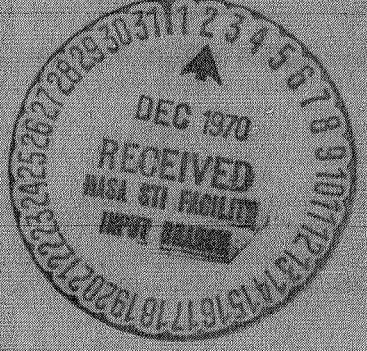

DEPOSITION OF ION THRUSTER EFFLUENTS ON SERT II SPACECRAFT SURFACES

by J. V. Staskus and Robert J. Burns

Lewis Research Center

Cleveland, Ohio 44135

NATIONAL AERONAUTICS AND SPACE ADMINISTRATION • WASHINGTON, D. C. • NOVEMBER 1970

1. Report No.	2. Government Accession No.	3. Recipient's Catalog No.
NASA TM X-2084		

4. Title and Subtitle	5. Report Date
DEPOSITION OF ION THRUSTER EFFLUENTS ON SERT II SPACECRAFT SURFACES	November 1970
	6. Performing Organization Code

7. Author(s)	8. Performing Organization Report No.
J. V. Staskus and Robert J. Burns	E-5805
	10. Work Unit No. 704-00

9. Performing Organization Name and Address	11. Contract or Grant No.
Lewis Research Center National Aeronautics and Space Administration Cleveland, Ohio 44135	

12. Sponsoring Agency Name and Address	13. Type of Report and Period Covered
National Aeronautics and Space Administration Washington, D.C. 20546	Technical Memorandum
	14. Sponsoring Agency Code

15. Supplementary Notes

16. Abstract

An experiment aboard the SERT II spacecraft to detect surface contamination by mercury ion thruster effluents is discussed. Two solar-cell sensors were located adjacent to each thruster, downstream from the exhaust plane. Sensor short-circuit current was the contamination sensitive parameter. One sensor at 60° C was for detection of sputtered thruster accelerator grid material (Mo), and the other sensor at -40° C was used for detection of propellant (Hg) and molybdenum. Flight data indicate that contamination of both sensors was due to molybdenum. Contamination of the low-temperature sensor by mercury was negligible. Radiation intensity transmitted by the contaminant film was reduced to 50 percent of the incident intensity within 6 to 12 hours of thruster startup.

17. Key Words (Suggested by Author(s))	18. Distribution Statement
Electric propulsion; mercury bombardment thruster; accelerator grid sputtering (or erosion); spacecraft surface contamination; solar array surface contamination; contamination sensors; thin films; optical transmission; solar array contamination	Unclassified - unlimited

19. Security Classif. (of this report)	20. Security Classif. (of this page)	21. No. of Pages	22. Price*
Unclassified	Unclassified	20	$3.00

*For sale by the Clearinghouse for Federal Scientific and Technical Information
Springfield, Virginia 22151

DEPOSITION OF ION THRUSTER EFFLUENTS ON SERT II SPACECRAFT SURFACES

by J. V. Staskus and Robert J. Burns

Lewis Research Center

SUMMARY

An experiment aboard the SERT II spacecraft to detect surface contamination by mercury ion thruster effluents is discussed. Two solar-cell sensors were located adjacent to each thruster downstream from the exhaust plane. Sensor short-circuit current was the contamination sensitive parameter. One sensor at 60° C was used for detection of sputtered thruster accelerator grid material (Mo), and the other sensor at -40° C was used for detection of propellant (Hg) in addition to molybdenum. Flight data indicate that contamination of both sensors was due to molybdenum. Contamination of the low temperature sensor by mercury was negligible. Radiation intensity transmitted by the contaminant film was reduced to 50 percent of the incident intensity within 6 to 12 hours of thruster startup.

INTRODUCTION

The SERT II spacecraft was launched on February 3, 1970, from Vandenberg Air Force Base onto the Western Test Range. The mission objective was to endurance test a mercury electron bombardment ion thruster (ref. 1) for a minimum of 6 months. Two thrusters were operated one at a time with power provided by a solar cell array. The orbit was 1000 kilometers, nearly circular, and inclined at 99°. The orbit was nearly Sun synchronous so that the solar array was exposed to continuous sunlight for a minimum of 6 months.

This report discusses an experiment to monitor the contamination of spacecraft surfaces downstream from the exhaust plane of the SERT II ion thruster. Neutral propellant (Hg) and sputtered accelerator material (Mo) are possible contaminants. The subject is of interest because of the electrical, thermal, optical, and chemical effects ion thruster effluents can have on spacecraft surfaces and systems. Accumulation of metals, sputtered or condensed, could bridge insulators in solar arrays, power distribution systems, or adjacent thrusters. The affected system would suffer a reduction in

performance or be rendered inoperative. Chemical reaction of other possible thruster effluents, notably cesium, severely degrades insulation (ref. 2). Thermal control of spacecraft is impaired by a contaminant coating on surfaces or by chemical reaction of the contaminant with the surface material. Opaque contamination of solar cell surfaces results in loss of spacecraft power.

The results of a study considering the above effects are discussed in reference 2. Contamination by mercury-ion-thruster propellant was treated theoretically in reference 3. Contamination by sputtered thruster material was also investigated experimentally in reference 4. The tests of reference 4 were performed in a 7.6-meter-diameter vacuum facility using a 1.5-meter-diameter mercury ion thruster and SERT II type of contamination sensors. Independent investigations of accelerator grid erosion produced particle emission rates but neglected the spatial distribution of the escaping particles.

The SERT II experiment provides the first flight measurement of mercury ion thruster efflux contamination on nearby spacecraft surfaces. It also provides a comparison to determine the applicability of the results of ground-based experiments to flight conditions. The flight data consisted of a voltage proportional to the solar radiation intensity transmitted by the contaminant film.

BACKGROUND

The experiment simulated solar array equilibrium temperature at 1 and 2 astronomical units (AU). Calculations indicate that a solar array front surface temperature is approximately 60° C at 1 AU and -40° C at 2 AU. Propellant condensation is possible whenever the arrival flux is greater than the evaporation rate shown in figure 1. The

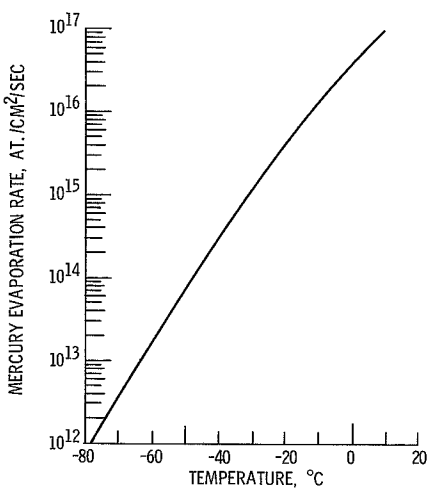

Figure 1. - Mercury evaporation rate as function of temperature.

arrival flux at the SERT II sensors is calculated using the following formula (ref. 5).

$$\mu = \nu_o \frac{xz}{2(x^2 + y^2)} \left\{ \frac{x^2 + y^2 + z^2 + r_o^2}{\sqrt{\left(x^2 + y^2 + z^2 + r_o^2\right)^2 - 4r_o^2(x^2 + y^2)}} - 1 \right\} \tag{1}$$

where

μ arrival flux at sensors, at./(cm^2)(sec)

ν_o exit flux from thruster = $\dfrac{\left(\frac{1}{\alpha} - 1\right)I_5}{\pi r_o^2 q}$ at./(cm^2)(sec)

x, y, z coordinates of sensor center with thruster accelerator grid center as the origin (see fig. 2)

r_o exhaust radius of thruster, 6.78 cm

α propellant utilization efficiency, 0.77

I_5 ion beam current, 0.253 A

q unit charge, 1.6×10^{-19} C

The arrival flux is found to be 5.62×10^{13} mercury atoms per square centimeter per second for the -40° C sensor (low-temperature sensor) and 5.39×10^{13} mercury atoms per square centimeter per second for the 60° C sensor (high-temperature sensor). The

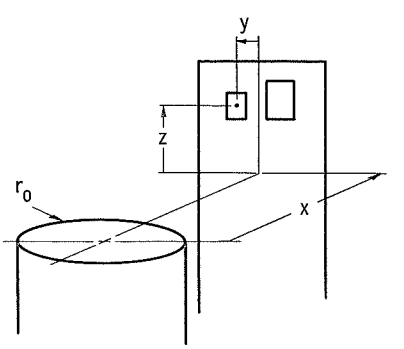

SENSOR	COORDINATE, CM		
	x	y	z
LOW TEMPERATURE	29.39	4.67	16.1
HIGH TEMPERATURE	30.96	3.58	15.28

Figure 2. - Coordinate definition and values for use in equation (1).

evaporation rate of mercury is 3×10^{14} atoms per square centimeter per second at -40° C. Therefore, condensation of mercury on the low temperature sensor at -40° C is critically dependent on the particle distribution. Mercury condensation will not occur on the high-temperature sensor at 60° C.

The situation regarding molybdenum contamination is quite different. Ground tests reported in reference 4 resulted in deposition of accelerator grid material at 1 to 2.5 monolayers per hour (4.44 to 11.1×10^{11} at./(cm^2)(sec)). Table I compares the ground

TABLE I. - COMPARISON OF SERT II PARAMETERS

WITH GROUND TEST PARAMETERS

	Ground test ref. 4	SERT II
Thruster radius, R, m	0.75	0.068
Beam current density, A/m^2	5.7	17.2
Neutral mercury efflux rate, at./(cm^2)(sec)	3.6×10^{15}	3.27×10^{15}
Distance from thruster exit to experimental solar cells, L, m	4.21	0.353
Length to radius ratio, L/R	5.63	5.19
Angle from thruster centerline to solar-cell experiment, deg	57	62.6
View factor, ratio of flux arriving at solar cell to flux leaving thruster exit, F	0.019	0.0168

test parameters with the SERT II parameters. A calculation using the relation (ref. 4)

$$\mu_1 = F\,\frac{If(3600)}{qA_o\sigma} \tag{2}$$

where

μ_1 arrival rate, monolayers/hr

F view factor μ/ν_o for cosine distribution from thruster exit to solar cell location; 0.0172 for low-temperature sensor, 0.0165 for high-temperature sensor

I ion beam current, 0.253 A

f fraction of primary ion current converted to charge exchange current, 0.00327

q 1.6×10^{-19} coulombs per unit charge

A_o thruster cross-section area, 145 cm^2

σ monolayer concentration (1 monolayer $\sim 1.6\times10^{15}$ at./cm^2)

predicts an accumulation rate of approximately 1.37 monolayers per hour for SERT II due to sputtered molybdenum. Using this result and the data from reference 6 regarding the optical transmission of thin silver films, a graph of transmission against time was generated (fig. 3). Since data on the transmission of thin molybdenum films was not

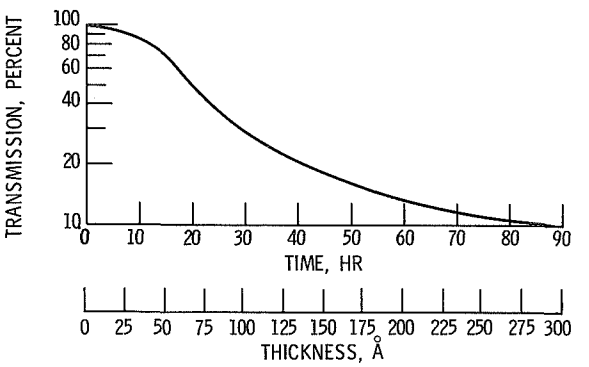

Figure 3. - Predicted transmission as function of time using equations (1) and (2) and reference 5. Thickness scale taken directly from reference 5.

available, it was assumed that the transmission against thickness for molybdenum was approximately the same as that for silver.

INSTRUMENTATION

A high- and a low-temperature sensor were mounted next to each other near the top of a large radiator facing the Sun and a thruster. Systems 1 and 2 sensors were located adjacent to thrusters 1 and 2, respectively (fig. 4). Each contamination sensor consisted of a series-connected group of solar cells whose output was dissipated in a resistive load. Short-circuit current is the parameter most sensitive to changes in input intensity and least sensitive to thermal variations. The load was, therefore, chosen to intersect the sensor characteristic on the short circuit current plateau (fig. 5).

The high- and low-temperature sensors were located at 63.7^o and 61.6^o from the beam axis and 36.8 and 33.8 centimeters, from the accelerator grid center, respectively (fig. 4). The low-temperature (LT) sensor was bonded to the radiator and the

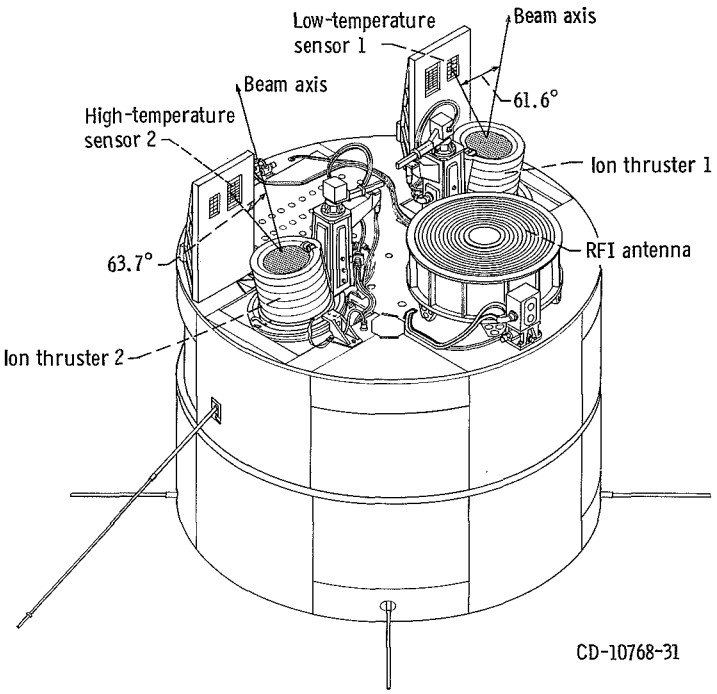

Figure 4. - SERT II spacecraft showing contamination sensor locations.

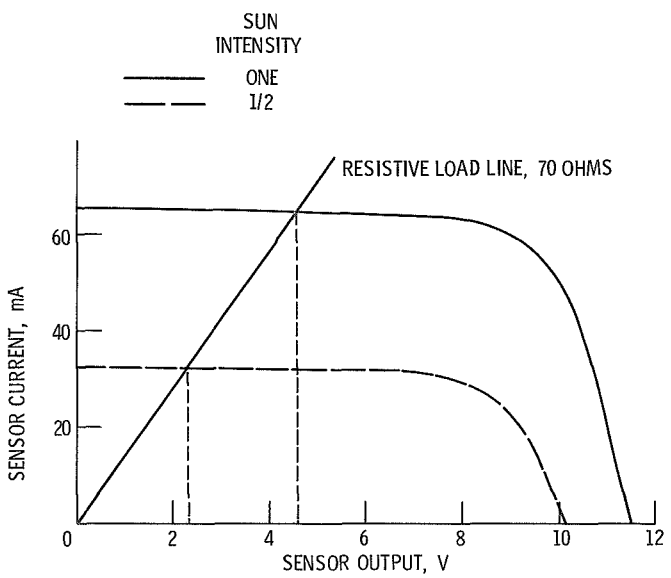

Figure 5. - High-temperature sensor characteristics.

high temperature (HT) sensor was suspended on polyester cords for thermal isolation from the radiator. Behind each sensor was a thermistor to monitor the sensor temperature. A reflective blanket on the structure and insulating mounts reduced the thermal input from the Sun and spacecraft. A more detailed description of the experiment is contained in appendixes A and B.

RESULTS AND DISCUSSION

The contamination experiment began operation as soon as the spacecraft was oriented so that the contamination sensors faced the Sun. Data were thus obtained prior to ion thruster operation. These data are shown in figure 6. Only data for system 2 are shown. However, the data from both systems were similar.

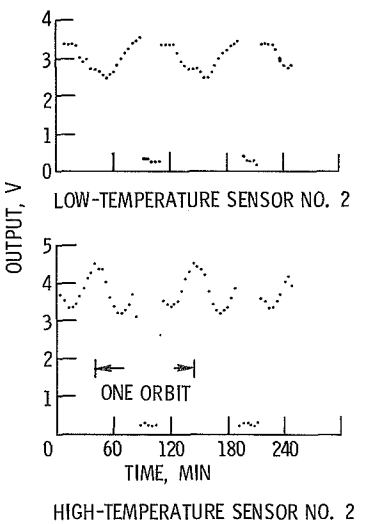

Figure 6. - Contamination sensor output voltages prior to thruster startup.

Figure 6 shows a periodic oscillation of the sensor outputs at the orbit frequency (1/105 min). Part of the variation was determined to be due to shadowing of the sensors by the top of the thruster and a radio-frequency interference experiment antenna (fig. 4). Shadowing occurred over 25 to 30 percent of the orbit in the southern hemisphere and was a result of the solar radiation being incident 26° from the orbit normal (fig. 7). As can be seen from the figure, no shadowing occurred over the northern hemisphere. The data also indicate that reflection from the top of the thruster to the sensors may have

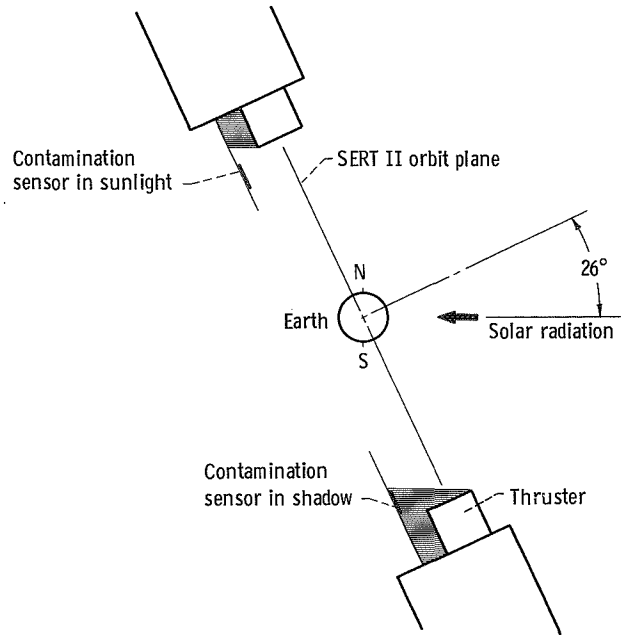

Figure 7. - Illustration of ion thruster shadowing contamination sensor over part of southern hemisphere.

occurred over the northern hemisphere. This is evidenced by the leveling of the output voltages of the low temperature sensor at 40 and 140 minutes (fig. 6).

System 2 Results

Thruster 2 was operated first. The thruster was brought to full thrust operation (253 mA beam current) in three steps. It was operated at an 88-milliampere beam current for 19.4 hours, then a 203 milliampere beam current for 6.8 hours, and full beam for 11.7 hours. The thruster was then shut down in preparation for operation of the prime thruster. Data from the associated contamination experiment are shown in figures 8 and 9.

Figure 8 shows the transmission and temperature for the low-temperature sensor as a function of time for the 38 hours of thruster operation. The transmission is the normalized sensor output voltage multiplied by 100. Only the maximum voltage values, which occurred once per orbit, were used; thus the oscillations due to shadowing and reflection are omitted. As is seen, the transmission decays rapidly with time, reaching 50 percent in 7.5 hours. The temperature was nearly constant at -40° C. The constant temperature eliminated the necessity for any temperature correction to the voltage data

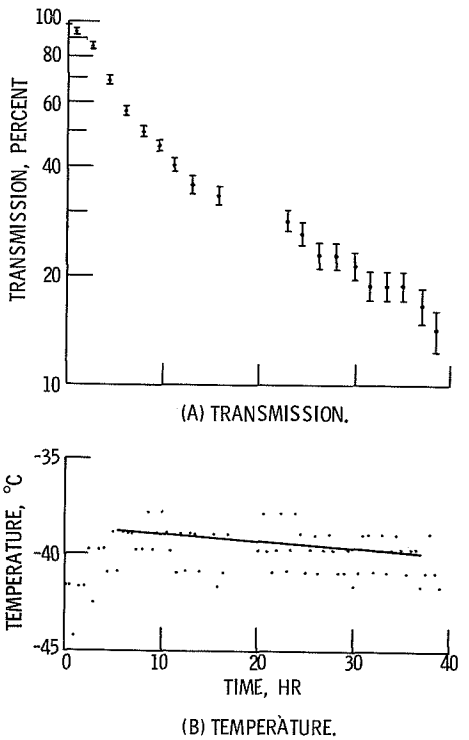

Figure 8. - System 2 low-temperature sensor transmission and temperature as function of time from thruster startup.

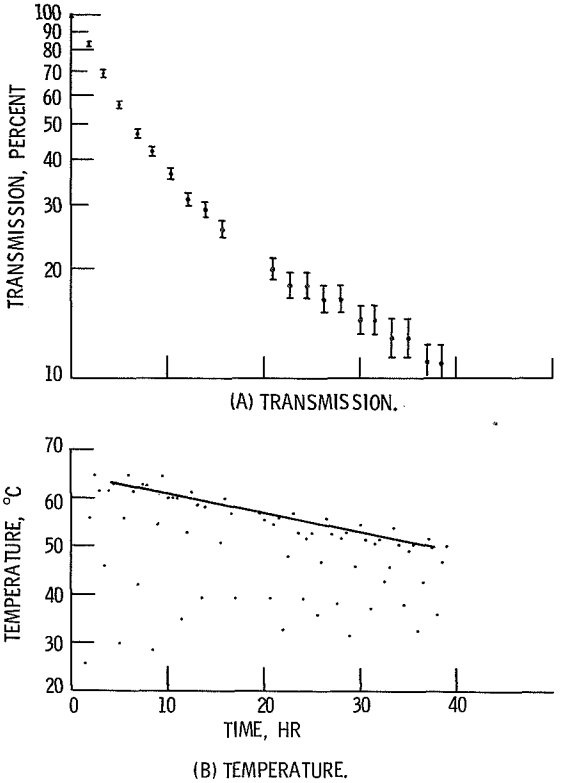

Figure 9. - System 2 high-temperature sensor transmission and temperature as function of time from thruster start-up.

before comparing transmission data with the predicted graph of transmission against time.

Figure 9 shows the transmission and temperature for the high-temperature sensor. As was the case with the low-temperature sensor, transmission decreases rapidly with time, reaching 50 percent in 6.5 hours. The temperature data indicate that rather large temperature variations occurred. Detailed analysis of the data shows that the sensor temperature was lowest for the 20 to 30 minutes that the sensor was being shadowed over the southern hemisphere. The temperature was a maximum when the output voltage was a maximum (i.e., unshadowed) over the northern hemisphere and varied little from orbit to orbit. This eliminated any requirement for temperature correction to the voltage data before comparing transmission data with the predicted graph of transmission against time. Comparison of the flight results (figs. 8(a) and 9(a)) with the results expected using equations (1) and (2) (fig. 3) shows that the transmission decayed more rapidly than predicted. The reason for this is unknown; however, the prediction was obtained with the assumption that

(1) Equation (1) gives an accurate description of the sputtered particle distribution.

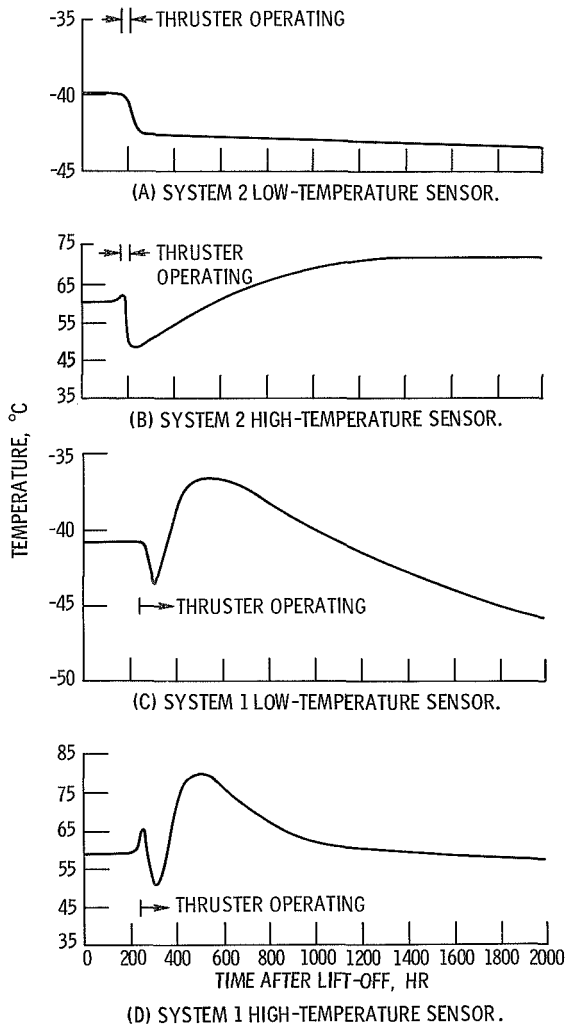

Figure 10. - System 2 sensor temperatures as function of time from SERT II lift-off.

(2) The f appearing in equation (2) is not a function of beam current.

(3) The transmission of molybdenum thin films is the same as the transmission of silver thin films of the same thickness.

It is possible that one or more of these assumptions are not valid.

Attempts were made to correlate the rate of transmission decay with ion-beam current variations. However, as is seen in figures 8(a) and 9(a), the results showed wide variations that are not consistent with the view that the transmission should decrease proportionate to increasing ion beam current. The reasons for this are as yet unknown. Further tests are necessary to remove the inconsistency.

It is noted that, in general, the high-temperature sensor transmission decayed more rapidly than the low-temperature sensor transmission. This suggests a lower rate of contamination for the low-temperature sensor. Consideration of the view factors μ/ν_o for the two sensors and the possible contamination mechanisms leads one to expect just the opposite to occur. The decay rate of the low-temperature sensor transmission as a result of molybdenum accumulation, should be slightly higher than the rate for the high-temperature sensor transmission. The addition of any mercury deposits on the low-temperature sensor should result in its transmission decaying even more rapidly than the high-temperature transmission.

Further investigation is required to produce a satisfactory explanation for the discrepancy between the high- and low-temperature sensor contamination rates. However, it was concluded, from the fact that the decay rate of the low-temperature sensors was not greater than the decay rate for the high-temperature sensors, that no significant mercury contamination occurred.

When the thruster was initially turned on, the temperatures of the high- and low-temperature sensors decreased for about 40 hours. The temperatures then began increasing (fig. 10). The temperature variations were concluded to be due to the deposition of material on the sensors. The deposits initially caused small decreases in the solar absorptance α and this caused the sensor temperatures to decrease. As the deposit thickness increased, more rapid decreases in the emittance ϵ were obtained. The resultant increase in the absorptance-emittance ratio α/ϵ caused the temperature of the sensors to increase. As figure 10(b) shows, the high-temperature sensor temperature increased following thruster 2 shutdown. This increase was due to a gradual decrease in the solar incidence angle from its initial value of 26°.

System 1 Results

Figures 11 and 12 show the transmission and temperatures as a function of time for the system 1 contamination sensors after thruster 1 startup. The thruster was operated

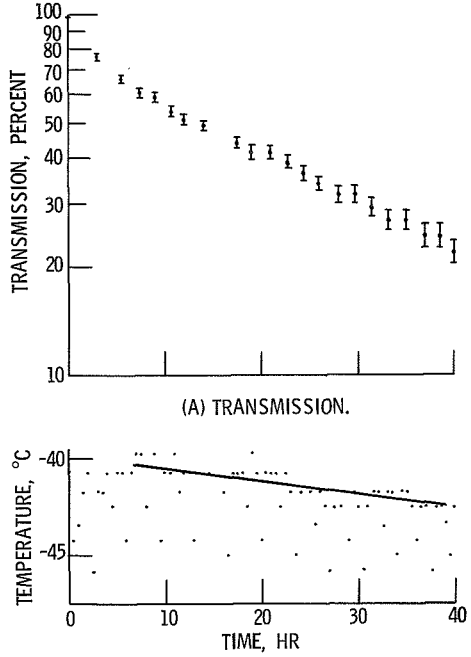

Figure 11. - System 1 low-temperature sensor transmission and temperature as function of time from thruster start-up.

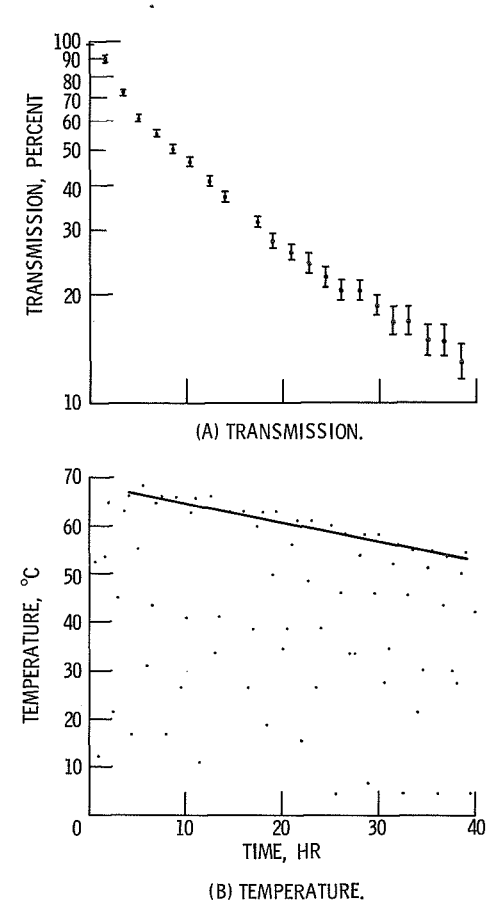

Figure 12. - System 1 high-temperature sensor transmission and temperature as function of time from thruster start-up.

at a 94 milliampere beam current for 3.9 hours and at a 203 milliampere beam current for 1.93 hours. Operation then continued at full beam (253 mA) beyond the lifetime of the contamination experiment. The results obtained are similar to those obtained for system 2. The transmission decreased 50 percent in 12 and 8.8 hours for the low- and high-temperature sensors, respectively. As with system 2, the low-temperature sensor transmission decayed more slowly than the high-temperature sensor transmission, and both decayed faster than predicted. Also, the system 1 results showed the same wide variation with ion beam current as obtained with system 2.

The decay rates for the system 2 sensors were initially higher than those of the system 1 sensors. It was concluded that the system 2 sensors were being contaminated at a slightly higher rate. The accelerator grid sputtering rate is dependent on the flux of ions impinging on the grid. The accelerator drain current is a measurement of this flux. The thruster data indicated that the system 2 accelerator drain current was 1.75 milliamperes compared with 1.60 milliamperes for system 1. This is consistent with the higher contamination rate of the system 2 sensors compared to the system 1 sensors.

CONCLUSION

Flight data showed considerable contamination. Contamination thickness reached 50-percent opacity in 7.5 to 12 hours for the sensors at -40° C and 6.5 to 8.8 hours for the sensors at 60° C. It was concluded that the contamination was caused by sputtered ion thruster grid material (Molybdenum). Contamination by neutral propellant (mercury) was negligible. Analysis indicated that the high-temperature-sensor transmission should decay more slowly than the low-temperature-sensor transmission. The apparent discrepancy between the contamination rate of the low-temperature sensor and that of the high-temperature sensor has not yet been explained.

Attempts were made to correlate the contamination rates with thruster operating parameters. No consistent correlations could be obtained. Thus, predictions of contamination rates from thruster operating parameters and receptor location requires further investigation of thruster efflux distribution. Data on the transmission of molybdenum thin films are needed. With these data it may be possible to detect differences in contamination rate attributable to different thruster beam currents.

Lewis Research Center,
National Aeronautics and Space Administration,
Cleveland, Ohio, July 27, 1970,
704-00.

APPENDIX A

SENSORS

The contamination sensors were basically groups of series-connected solar cells. The low temperature sensor consisted of 10, 1- by 2-centimeter silicon N on P solar cells. The 0.033-centimeter-thick cells had a base resistivity of 2 ohm-centimeters. The short-circuit current was 65 milliampere ±5 percent at 25° C with one solar constant radiation input. The temperature coefficient of the short circuit current was no greater than 0.1 milliampere per °C. The cover glasses were 0.051-centimeter 7940 fused silica with a standard blue coating; adhesive was RTV 602. Two adjacent rows of cells were fixed to a 0.013-centimeter insulating sheet which was then bonded to a 0.13 centimeter stainless-steel substrate. This assembly was then bonded to the radiator of the structure. The high temperature sensor consisted of 3 rows of 7 cells each. The materials and assembly were the same as that of the low-temperature sensor. The high-temperature sensor contained more solar cells than the low temperature sensor since it was required to produce the same output at a higher temperature. Cell efficiency decreases with increasing temperature.

Four telemetry channels were required for each experiment. These were used to monitor the outputs from the high- and low-temperature sensors as well as sensor temperatures. Each parameter was sampled once every 4 minutes and recorded as 0 to 61 counts for a 0 to 5 volt telemetry voltage (0.082 v/count). The sensor output consisted of the voltage produced across a load resistor in series with the sensor (fig. 13). The resistor was chosen such that its load line intersected the sensor I-V characteristic on the portion proportional to short circuit current (fig. 5). Short-circuit current was chosen as the sensitive parameter because it is most sensitive to variations in incident radiation intensity and least sensitive to temperature changes. The output was routed directly to the telemetry system with no intervening signal conditioning.

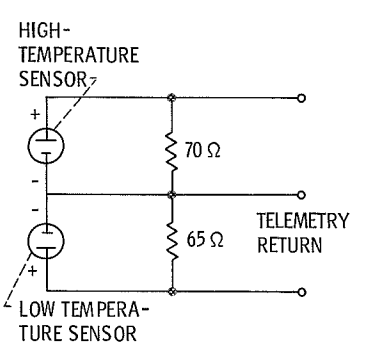

Figure 13. - Sensor circuits.

Temperature compensation was not necessary since the sensor's temperature varied slowly compared with the rate of contamination and the effect on the output was small. The temperature would have to change by 11^{o} C before the output voltage variation would exceed the resolution of the telemetry system. Each sensor did, however, have a thermistor mounted behind it to monitor temperature changes. Thermistors for the temperature ranges of 0^{o} to 80^{o} C and -75^{o} to -30^{o} C were required. Temperature measuring circuitry is shown in figure 14. It should be noted that the temperature indicated by the thermistor was probably lower than the front surface of the solar cell cover glass. This is because 2.8 and 4.1 millimeter of glass, adhesives, silicon, and metal separated the thermistor from the glass front surface. Calculations indicated the difference to be on the order of 2^{o} to 3^{o} C. The effect on the accumulation of sputtered molybdenum on the sensors should be negligible but it does require that the arrival rate of neutral mercury be approximately 5×10^{14} atoms per square centimeter per second rather than 3×10^{14} atoms per square centimeter per second before mercury accumulation occurs.

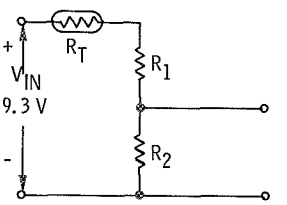

SENSOR	R_1, Ω	R_2, Ω	R_T Ω AT 25° C
LOW TEMPERATURE	6.98 K	15 K	100 K
HIGH TEMPERATURE	13.7 K	30 K	500 K

Figure 14. - Temperature measurement circuits.

APPENDIX B

STRUCTURE

The experiment structure is an open rectangular pyramid of riveted aluminum construction (fig. 15). It consists primarily of a 27.9 by 50.8-centimeter plate which is oriented perpendicular to the top of the spacecraft and facing the sun (fig. 4). This plate serves as a radiator for the low-temperature sensor and provides a support structure for both sensors. The sensors are mounted next to each other near the top of the radiator. The low-temperature sensor is dispersed from the ion beam axis by 61.6° and is 33.8 centimeters from the center of the thruster accelerator grid. The high-temperature sensor is 63.7° from the beam axis and 36.8 centimeters from the grid center. The low-temperature sensor is bonded directly to the radiator and the high-temperature sensor is thermally isolated from the radiator. Isolation is achieved by suspending the sensor behind a hole cut in the radiator.

Suspension of the high-temperature sensor is provided by a 24-pound (10.9-kg),

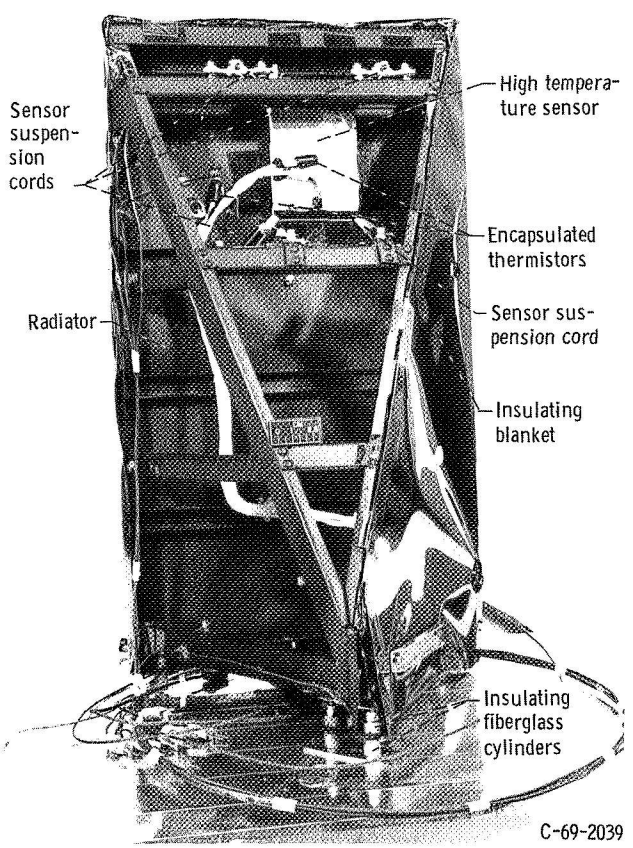

Figure 15. - Contamination experiment structure.

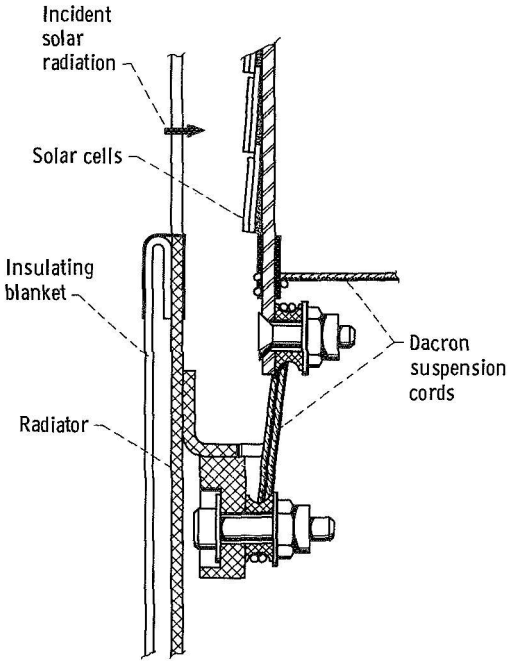

Figure 16. - High temperature sensor mounting detail.

480 filament, Dacron cord (fig. 16). Dacron was chosen for its low thermal conductivity, high strength, and acceptable creep properties. Provision was made for periodic manual tightening of the suspension prior to flight to compensate for relaxation of the Dacron with time under load.

Thermal conduction from the spacecraft is minimized by mounting the experiment on fiberglass cylinders (fig. 17). Thermal radiation from the sun and top of the spacecraft is minimized by covering the front of the radiator and one side of the structure with a reflective blanket. The blanket is composed of 20 layers of randomly wrinkled, aluminized, 0.0038-millimeter Mylar with two cover sheets of 0.013 millimeter aluminized Kapton. A final 0.13 millimeter aluminized Kapton front cover provides support and protection for the blanket. The Mylar is wrinkled to minimize the contact between sheets

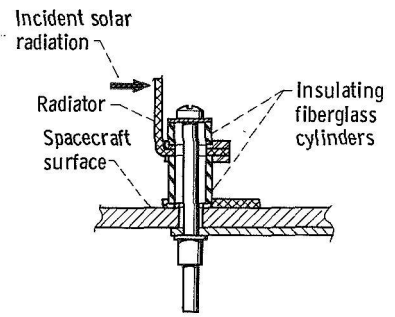

Figure 17. - Experiment mounting.

and prevent heat transfer by conduction. To prevent electrostatic charge accumulation on the aluminized surfaces, a multifingered aluminized Kapton strap attached to each layer of the blanket provides a ground circuit to the spacecraft. The materials and fabrication techniques used were similar to those used to build the Apollo Lunar Module multilayer insulation blanket (ref. 7). A complete experiment weighed 2.1 kilograms.

Structural surfaces not covered by the thermal blanket were painted with black paint having an emittance of 0.88. The rear surface of the high-temperature sensor was 85 percent aluminum foil tape and 15 percent black paint to maintain it at approximately $+55^{\circ}$ C. (The emittance of the aluminum tape is 0.06.)

Temperature predictions for various thermal control methods were made with a 32-node analytical model of the contamination experiment using the Chrysler Improved Numerical Differencing Analyzer (CINDA) program. Heat interchange between the superinsulating blanket and the main structure was computed as a radiation conductor using an effective emittance of 0.01. Radiation losses to the environment were tailored to account for the side blockage due to the wrap-around of the blanket. The model was calibrated against experimental data obtained in the solar simulation qualification and flight acceptance tests. The data were used to analytically adjust the conductance paths to the high-temperature sensor (heat conducted through the Dacron cords) as well as the heat loss through the mounting bolts. The flight temperature predictions were generated using the analytical model coupled to the analytical model of the thruster. Environmental heating was limited to solar and Earth thermal to the Sun side and Earth thermal to the shade side. Albedo heating was neglected. Radiation heat interchange between the thruster and both of the sensors was included in the model. The shading of the insulating blanket by the thruster was also included. Using this model, the temperature predictions along with initial flight results are given in table II.

TABLE II. - COMPARISON OF PREDICTED SENSOR TEMPERATURES WITH FLIGHT RESULTS

Sensor	Temperature, $^{\circ}$C	
	Predicted	Achieved
Low temperature No. 1	-54.4	$-37.6^{+4.2}_{-1.4}$
High temperature No. 1	57.2	$61.3^{+4}_{-1.2}$
Low temperature No. 2	-54.4	$-40.8^{+4.2}_{-1.4}$
High temperature No. 2	57.8	$62.8^{+4}_{-1.2}$

REFERENCES

1. Kerslake, William R.; Byers, David C.; and Staggs, John F.: SERT II Experimental Thrustor System. Paper 67-700, AIAA, Sept. 1967.

2. Hall, D. F.: Evaluation of Electric Propulsion Beam Divergence and Effects on Spacecraft. Rep. 08965-6013-RO-00, TRW, Inc., Sept. 1969.

3. Staggs, John F.; Gula, William P.; and Kerslake, William R.: The Distribution of Neutral Atoms and Charge-Exchange Ions Downstream of an Ion Thrustor. Paper 67-82, AIAA, Jan. 1967.

4. Richley, Edward A.; and Reynolds, Thaine W.: Condensation on Spacecraft Surfaces Downstream of a Kaufman Thruster. NASA TM X-52746, 1970.

5. Lozgachev, V. I.: Distribution of Molecular Flow on a Surface During Evaporation in Vacuum. Soviet Phys. - Tech. Phys., vol. 7, no. 8, Feb. 1963, pp. 736-744.

6. Holland, L.: Vacuum Deposition of Thin Films. John Wiley & Sons, Inc., 1956, p. 245.

7. Bartilucci, A.; Lee, E.; and Tawil, M. N.: LM Passive Thermal Design and Test. Paper 68-748, AIAA, June 1968.

NASA-Langley, 1970 — 31 E-5805

NATIONAL AERONAUTICS AND SPACE ADMINISTRATION
WASHINGTON, D.C. 20546

OFFICIAL BUSINESS

FIRST CLASS MAIL

POSTAGE AND FEES PAID
NATIONAL AERONAUTICS AN
SPACE ADMINISTRATION

POSTMASTER: If Undeliverable (Section 158
Postal Manual) Do Not Retur

"The aeronautical and space activities of the United States shall be conducted so as to contribute . . . to the expansion of human knowledge of phenomena in the atmosphere and space. The Administration shall provide for the widest practicable and appropriate dissemination of information concerning its activities and the results thereof."

—NATIONAL AERONAUTICS AND SPACE ACT OF 1958

NASA SCIENTIFIC AND TECHNICAL PUBLICATIONS

TECHNICAL REPORTS: Scientific and technical information considered important, complete, and a lasting contribution to existing knowledge.

TECHNICAL NOTES: Information less broad in scope but nevertheless of importance as a contribution to existing knowledge.

TECHNICAL MEMORANDUMS: Information receiving limited distribution because of preliminary data, security classification, or other reasons.

CONTRACTOR REPORTS: Scientific and technical information generated under a NASA contract or grant and considered an important contribution to existing knowledge.

TECHNICAL TRANSLATIONS: Information published in a foreign language considered to merit NASA distribution in English.

SPECIAL PUBLICATIONS: Information derived from or of value to NASA activities. Publications include conference proceedings, monographs, data compilations, handbooks, sourcebooks, and special bibliographies.

TECHNOLOGY UTILIZATION PUBLICATIONS: Information on technology used by NASA that may be of particular interest in commercial and other non-aerospace applications. Publications include Tech Briefs, Technology Utilization Reports and Notes, and Technology Surveys.

Details on the availability of these publications may be obtained from:

SCIENTIFIC AND TECHNICAL INFORMATION DIVISION

NATIONAL AERONAUTICS AND SPACE ADMINISTRATION

Washington, D.C. 20546